

Silicon-based plasmonic waveguides

Alexey V. Krasavin* and Anatoly V. Zayats

Centre for Nanostructured Media, IRCEP, The Queen's University of Belfast, Belfast, BT7 1NN, UK

*a.krasavin@qub.as.uk

Abstract: We propose and comprehensively investigate Si-based plasmonic waveguides as a means to confine and manipulate photonic signals. The high refractive index of Si assures strong confinement and a very high level of photonic integration with achievable waveguide separations of the order of 10 nm and waveguide bends with 500 nm radius at telecommunication wavelengths, while using Al and Cu plasmonic material platforms, makes such waveguides fully compatible with existing CMOS fabrication processes. Their potential future in hybrid electronic/photonic chips is further reinforced as various configurations have been shown to compensate SPP propagation loss. The group velocity dispersion of such waveguides allows over 10 Tb/s signal transfer rates. The figures of merit allowing comparison of passive and active functionalities achievable with various waveguides have also been introduced.

©2010 Optical Society of America

OCIS codes: (250.5403) Plasmonics; (130.0130) Integrated optics.

References and links

1. M. Lipson, "Guiding, modulating, and emitting light on silicon - challenges and opportunities," *J. Lightwave Technol.* **23**(12), 4222–4238 (2005).
2. S. I. Bozhevolnyi, ed., *Plasmonic Nanoguides and Circuits* (Pan Stanford Publ., 2008).
3. J.-M. Lee, S. Park, M.-S. Kim, S. K. Park, J. T. Kim, J.-S. Choe, W.-J. Lee, M.-H. Lee, and J. J. Ju, "Low bending loss metal waveguide embedded in a free-standing multilayered polymer film," *Opt. Express* **17**(1), 228–234 (2009), <http://www.opticsinfobase.org/oe/abstract.cfm?URI=oe-17-1-228>.
4. J. Tian, S. Yu, W. Yan, and M. Qiu, "Broadband high-efficiency surface-plasmon-polariton coupler with silicon-metal interface," *Appl. Phys. Lett.* **95**(1), 013504 (2009).
5. P. Neutens, P. Van Dorpe, I. De Vlamincq, L. Lagae, and G. Borghs, "Electrical detection of confined gap plasmons in metal-insulator-metal waveguides," *Nat. Photonics* **3**(5), 283–286 (2009).
6. S. I. Bozhevolnyi, V. S. Volkov, E. Devaux, J.-Y. Laluet, and T. W. Ebbesen, "Channel plasmon subwavelength waveguide components including interferometers and ring resonators," *Nature* **440**(7083), 508–511 (2006).
7. M. Yan, and M. Qiu, "Guided plasmon polariton at 2D metal corners," *J. Opt. Soc. Am. B* **24**(9), 2333–2342 (2007).
8. S. A. Maier, "Plasmonics: metal nanostructures for subwavelength photonic devices," *J. Sel. Top. Quantum Electron.* **12**(6), 1214–1220 (2006).
9. G. A. Wurtz, W. Dickson, D. O'Connor, R. Atkinson, W. Hendren, P. Evans, R. Pollard, and A. V. Zayats, "Guided plasmonic modes in nanorod assemblies: strong electromagnetic coupling regime," *Opt. Express* **16**(10), 7460–7470 (2008), <http://www.opticsinfobase.org/oe/abstract.cfm?URI=oe-16-10-7460>.
10. A. V. Krasavin, and A. V. Zayats, "Three-dimensional numerical modeling of photonic integration with dielectric-loaded SPP waveguides," *Phys. Rev. B* **78**(4), 045425 (2008).
11. T. Holmgaard, Z. Chen, S. I. Bozhevolnyi, L. Markey, A. Dereux, A. V. Krasavin, and A. V. Zayats, "Wavelength selection by dielectric-loaded plasmonic components," *Appl. Phys. Lett.* **94**(5), 051111 (2009).
12. Z. Chen, T. Holmgaard, S. I. Bozhevolnyi, A. V. Krasavin, A. V. Zayats, L. Markey, and A. Dereux, "Wavelength-selective directional coupling with dielectric-loaded plasmonic waveguides," *Opt. Lett.* **34**(3), 310–312 (2009).
13. J. Grandidier, G. C. des Francs, S. Massenot, A. Bouhelier, L. Markey, J.-C. Weeber, C. Finot, and A. Dereux, "Gain-assisted propagation in a plasmonic waveguide at telecom wavelength," *Nano Lett.* **9**(8), 2935–2939 (2009).
14. D. O'Connor, M. McCurry, B. Lafferty, and A. V. Zayats, "Plasmonic waveguide as an efficient transducer for high-density data storage," *Appl. Phys. Lett.* **95**(17), 171112 (2009).
15. A. V. Krasavin, and A. V. Zayats, "All-optical active components for dielectric-loaded plasmonic waveguides," *Opt. Commun.* **283**(8), 1581–1584 (2010).
16. E. D. Palik, ed., *Handbook of Optical Constants of Solids* (Academic press, New York, 1984).
17. R. Buckley, and P. Berini, "Figures of merit for 2D surface plasmon waveguides and application to metal stripes," *Opt. Express* **15**(19), 12174–12182 (2007), <http://www.opticsinfobase.org/oe/abstract.cfm?URI=oe-15-19-12174>.

1. Introduction

Silicon photonics relies on the high refractive index of Si in the datacom spectral range to transmit optical signals in sub-wavelength size waveguides. Such waveguides and devices based on them would be crucial for the implementation of photonic interconnects and their integrated networks in electronics, where the electrical interconnect performance is a limiting factor for future developments. In most common Si-based configurations (channel waveguides with an effective refractive index $n_{eff} \sim 3$ or ridge waveguides with $n_{eff} \sim 2$) the waveguide cross-sectional dimensions are below or comparable to the transmitted light wavelength ensuring single mode guiding and a reasonably small mode size [1]. Even smaller photonic guides are achievable with surface plasmon polariton (SPP) based waveguides [2]. The use of plasmonic waveguides significantly reduces the mode size due to coupling to electron plasma oscillations near the metal interface. Moreover, it has the advantage of sending both electric and photonic signals along the same circuitry, thus naturally incorporating electronically controlled nodes in the plasmonic interconnect circuits.

Various types of plasmonic waveguides have been proposed, such as metallic stripe [3], gap [4,5], channel [6], and wedge SPP waveguides [7] as well plasmonic waveguides based on chains of metallic nanoparticles [8,9]. From the point of view of practical implementation, dielectric-loaded SPP waveguides (DLSPWs) deserve special attention, since they are formed by a dielectric ridge on the surface of a metal film and can be fabricated using industry-standard lithographic processes [10–14]. They provide an excellent trade-off between subwavelength confinement and the propagation loss associated with Ohmic losses in metal. This type of waveguide provides an additional opportunity to control plasmonic signals by modifying the properties of the dielectric forming the guide [14,15].

However, if DLSPW technology is to be introduced into CMOS circuitry, the materials used in DLSPW fabrication should be also compatible with the electronic chip fabrication process used at present. Silicon in this case is becoming one of the main candidates for the dielectric core of DLSPW. Moreover, the choice of such high refractive index material may allow further confinement of plasmonic modes, making DLSP components more compact and thus allowing higher density of integration. This, in turn, poses a new material problem of Au being incompatible with CMOS fabrication process, requiring the use of other plasmonic materials, for example Al or Cu.

In this article, using full-vectorial eigenmode simulations we study Si-based DLSP waveguides. We compare the performance of such Si-based plasmonic waveguides for different metals such as gold, aluminium or copper. Thus, we demonstrate a technologically feasible approach to implement subwavelength photonic circuits in electronic chips. Group-velocity dispersion (GVD) and gain in this type of plasmonic waveguides are also discussed. Furthermore, we introduce new figures of merits (FOMs) for the comparison of plasmonic waveguides in terms of their performance in active components (such as switches and modulators) and achievable density of integration.

2. SPP mode dispersion on Si-metal interface

We start by examining SPP dispersion and propagation length on a planar Si/metal interface with various semi-infinite metals (in practice the thickness of about 100 nm will be sufficient to achieve this approximation), shown in Fig. 1 by solid lines. The SPP dispersions show a typical behavior, following the light line at low frequencies and converging to the surface plasmon frequency at shorter wavelengths [Fig. 1(a)]. Please note that the light line for Si is curved due to the dispersion of the refractive index. SPP propagation on a Si/metal interface is much shorter than for corresponding frequencies of SPPs on air/metal interface even in the frequency range where Si is transparent. The primary reason for this is that due to high refractive index of silicon the SPP electromagnetic field is pushed into the metal, therefore, increasing Ohmic losses. The absorption in silicon plays only a secondary role even in the

visible spectral range ($L_{prop}^{\varepsilon=\varepsilon_{Si}} \approx L_{prop}^{\varepsilon=\text{Re}(\varepsilon_{Si})}$), since the Si absorption is not high enough to affect propagation of SPPs at the length scales of the order of tens micrometers. Although Au provides a shorter SPP wavelength than Al at a given frequency, the propagation length is about the same in both cases due to the interplay between the different degree of light confinement and Ohmic loss associated with these metals.

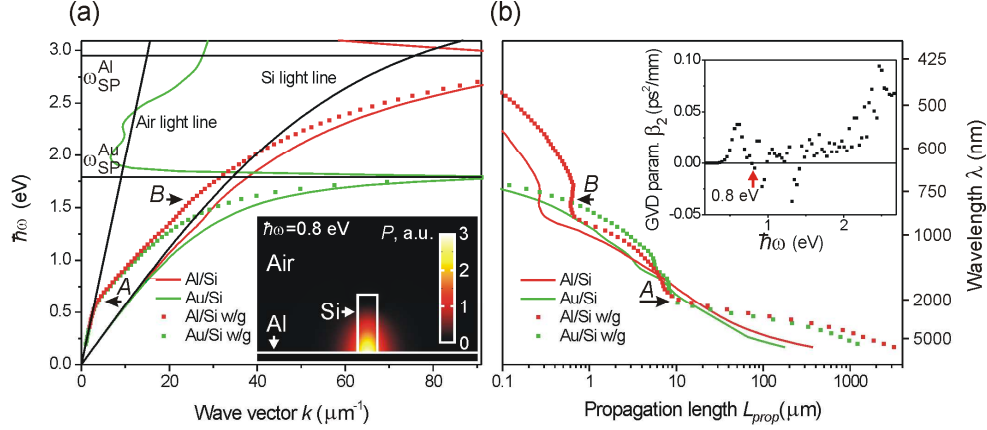


Fig. 1. (a) SPP dispersion and (b) propagation length for a semi-infinite Si/metal interface and for a TM_{00} mode in a $100 \times 300 \text{ nm}^2$ Si-based DLSP waveguide. The results are presented for aluminium and gold, the dielectric constants were taken from Ref. 16. Insets: in (a) the color map presenting the power flow along a $100 \times 300 \text{ nm}^2$ Si/Al waveguide for $\lambda = 1.55 \text{ }\mu\text{m}$ (0.8 eV); in (b) group velocity dispersion parameter β_2 as a function of frequency calculated for the same waveguide. Bends A and B of the dispersions are discussed in the text.

When a SPP waveguide is formed by, e.g., a $100 \times 300 \text{ nm}^2$ Si stripe of rectangular cross-section placed on a metal surface, guided SPP mode dispersion curves lie between the air light line and the SPP dispersion curve at a flat Si/metal interface, as should be expected. At wavelengths longer than $\sim 1100 \text{ nm}$ ($\sim 1.1 \text{ eV}$) the waveguide is singlemode, supporting only a fundamental TM_{00} SPP mode. At low frequencies it follows the SPP dispersion on the air/metal interface, being very close to the air/metal light line. This happens because the mode significantly extends out of the waveguide, therefore its dispersion is primarily influenced by the air/metal interface. This also leads to large propagation lengths [Fig. 1(b)]. Thus, at the frequencies corresponding to energy below 0.6 eV, the waveguide is in a weak guiding regime. As frequency is increased, the mode becomes more confined within the guide and the dispersion curve deviates from the air light line. Now the waveguide is in a true guiding regime with high effective refractive index. As the frequency increases further, the SPP mode dispersion curves pass the light line in silicon. Then, the mode becomes localized within the silicon ridge and the dispersion curve converges to the SPP dispersion at the silicon/metal interface. The general trend for the propagation length dependence is its decrease for higher frequencies. Both Si/Al and Si/Au waveguide modes have a bend in their dispersion at $\sim 0.6 \text{ eV}$ (bend A in Fig. 1) due to change in localization of the mode, described above. The bend at $\sim 1.6 \text{ eV}$ (bend B in Fig. 1) exists only for the Si/Al material pair (in both flat interface and waveguide configurations) corresponding to an interband absorption line in aluminium. Note, that although aluminium is not usually considered as a plasmonic material, its performance in terms of the propagation length at all frequencies is similar to the performance of gold for the reasons discussed above.

3. Si-SPP modes in the waveguides of different cross-sections

For further simulations, we choose the wavelength of $\lambda = 1.55 \text{ }\mu\text{m}$, relevant for telecommunication applications. At this wavelength both Si/Al and Si/Au based waveguides

provide very similar SPP effective refractive index and propagation lengths. As a next step, we investigated in more detail the guiding and confinement properties of Si/Al plasmonic waveguides, particularly addressing waveguides with essentially subwavelength dimensions of few hundreds of nanometres. At the waveguide cross-sections below $230 \times 230 \text{ nm}^2$ (well beyond the cut-off size for the fundamental TE_{00} photonic mode and TM_{10} , TM_{01} plasmonic modes which all appear above $\sim 320 \times 320 \text{ nm}^2$) the waveguide is singlemode supporting only a fundamental TM_{00} SPP mode, which will be the focus of this study. Generally, the performance of the waveguide is a trade-off between mode localization and its propagation wavelength. The particular ratio between these parameters essentially depends on the waveguide cross-section. To find the optimal cross-section, we performed a set of numerical simulations of a rectangular Si-SPP waveguide. Waveguide geometrical parameters [defined by its width w and height h , see an inset to Fig. 2(b)] were continually varied, while monitoring the guiding characteristics of the SPP mode (Fig. 2). When the waveguide dimensions are much smaller in comparison with half the wavelength of light in silicon ($\lambda n_{\text{Si}} = 223 \text{ nm}$), then the electromagnetic fields are pushed out of the waveguide [see the left field map in the inset to Fig. 2(b)], which leads to the effective refractive index of the mode n_{eff} being close to 1 [Fig. 2(a)], a large propagation length up to $100 \mu\text{m}$ [Fig. 2(b)] and rather large effective mode area S_{eff}^A [Fig. 2(c)].

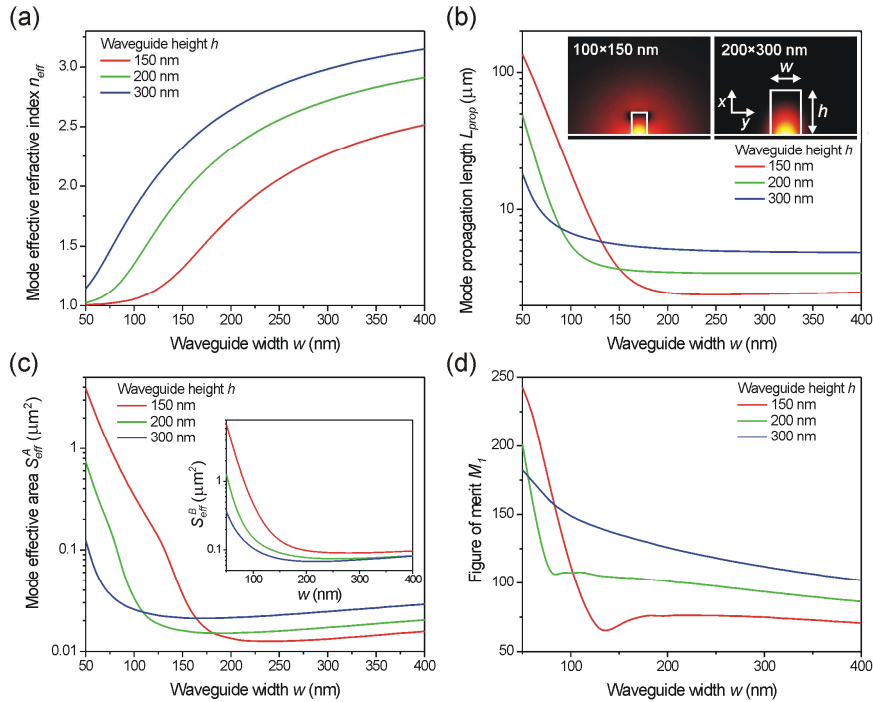


Fig. 2. a) Effective refractive index, (b) propagation length, (c) effective area, and (d) figure of merit M_f for Si-SPP mode as a function of waveguide width w and height h . Insets: Field maps presenting the absolute value of the power flow along the waveguide for waveguide cross-sections of $100 \times 150 \text{ nm}^2$ and $200 \times 300 \text{ nm}^2$.

When the width of the waveguide increases up to 200 nm and higher, the mode become more and more localized in the waveguide [see the right field map in the inset to Fig. 2(b)], its effective refractive index finally approaching that of a SPP mode on a plain Si/Al interface ($n = 3.56$). High contrast between the mode effective refractive index and the refractive index of the surrounding media ensure possibility of sharp waveguide bending, important for photonic integration. The effective mode area dramatically decreases, having a shallow

minimum at the waveguide width $w \sim 150\text{-}200$ nm, while the propagation length stabilizes in the region of ~ 5 μm , corresponding to ten SPP wavelengths. Here we note an interesting fact, in contrast with the tendencies described above; for wide waveguides the mode area and the propagation length decrease as the waveguide height changes from 300 nm (where it is close to the one at a planar Si/Al interface $L_{prop} \approx 7.8$ μm) to 150 nm [Figs. 2(b) and 2(c)]. This corresponds to the pattern for wide waveguides when the top polymer/air interface effectively push the fields into the metal, which then leads to the decrease of the mode area [Fig. 2(c)] and increase of losses due to the increased field confinement near the metal [Fig. 2(b)]. This remains correct up to waveguide height of several tens of nanometres.

The mode effective area was estimated using two approaches. In the first one, we carefully mapped the absolute value of power flow along the waveguide $|P_z|$ and found the area S_{eff}^A inside the constant level contour, encircling $(1-3e^{-2})$ part of the total $|P_z|$ integral [Fig. 2(c)]. This corresponds to the part of the intensity encircled by $1/e$ field decay contour in the case of the Gaussian distribution. We used an integral rather than a magnitude condition for the level defining the contour, because with various waveguide cross-sections, various mode decay dependencies should be expected. In this case the integral condition for the contour is more appropriate. The second approach we used is based on well known formula for mode area estimation $S_{eff}^B = \left(\int IdS \right)^2 / \int I^2 dS$, where I is the field intensity. The results for S_{eff}^B are presented in the inset to Fig. 2(c). Both approaches return very similar dependencies. To understand the trade-off between the mode confinement and propagation length, we introduced a figure of merit (FOM) $M_I = 2\sqrt{\pi} \cdot L_{prop} / \sqrt{S_{eff}^A}$, defined in a way similar to Ref. 17. Generally, for all the waveguide heights, M_I is a monotonically decreasing function of the waveguide width [Fig. 2(d)]. However, for small waveguide widths, the large effective mode area and the effective mode index close to the refractive index of the surrounding media are hardly compatible with the requirements of high-density photonic integration and result in strong losses at sharp waveguide bends.

4. Figures of merit

The figure of merit M_I provides an easy and quick outlook of the waveguide performance. However, to gain insight into the performance of the waveguides in terms of switching and modulation applications and achievable density of photonic integration, we have introduced modified FOMs. The square root of the mode area in the denominator of M_I is effectively a measure of how closely parallel waveguides can be packed on a chip. However, modes with the same effective areas can be coupled more efficiently or less efficiently to the neighboring waveguide depending on their spatial field distributions. Therefore, the figure of merit was modified in order to represent the coupling efficiency directly. When two parallel waveguides are placed next to each other, the coupling leads to the tunneling of the mode from one waveguide to another with a full energy transfer after a distance L_{coupl} [10]. As a criterion for cross-talk estimations, $L_{coupl} = 250$ μm was chosen for all waveguide cross-sections based on a typical propagation length for Si-SPP waveguides, so that after ~ 5 propagation lengths less than 1% of the energy will be coupled to the neighboring waveguide, which can be neglected. For each cross-section the waveguide centre-to-centre separation, d , satisfying this condition was found. In order to do this, an eigenmode problem is solved for the two coupled waveguides, and L_{coupl} is then determined as half a period of beating between symmetric and asymmetric modes in the system $L_{coupl} = \lambda / \left[2(n_{eff}^{sym} - n_{eff}^{asym}) \right]$. As a result, the first modification of the figure of merit $M_A = L_{prop} / d$ is obtained [Fig. 3(a)]. The general trends here are the same as for M_I , diverging from this behaviour as M_A starts to increase for wider waveguides. It can be explained by a faster decrease of the exponential tail in the horizontal direction than predicted by the average mode area estimation approach used in M_I . This leads to possible separation distances of the order of 10 nm for waveguides wider than ~ 350 nm.

Such separations are rather unrealistic from a fabrication point of view, and we introduced a minimum separation between the waveguides of 100 nm. This constraint is responsible for an abrupt change in the trends in the graphs at larger the waveguide widths.

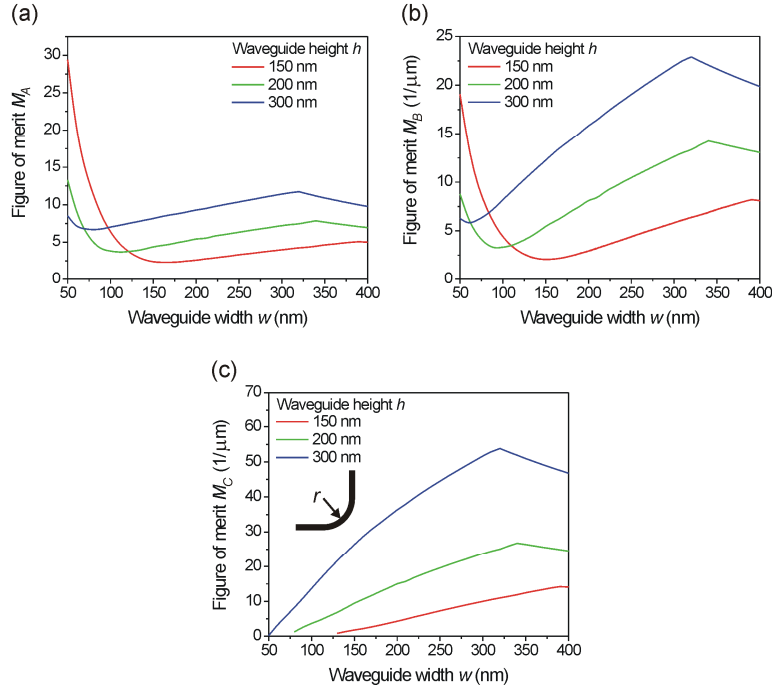


Fig. 3. Figures of merit for Si/Al SPP waveguide defined for monitoring performance with respect to (a) waveguide separation, M_A and (b) MZI and WRR functionalities, M_B . (c) M_C combines M_A , M_B , and bend radius performance. Please see the text for details.

Considering the performance of waveguide circuitry elements such as Mach-Zehnder interferometers (MZIs) and waveguide ring resonators (WRRs), it becomes apparent that not absolute L_{prop} but the mode propagation length expressed in terms of the mode wavelength $L_{prop}/(\lambda/n_{eff})$ is now the important parameter since it governs the phase-related effects achievable during the mode propagation. Following this considerations, the figure of merit is modified to be $M_B = L_{prop}n_{eff}/\lambda d$ [Fig. 3(b)]. In terms of density of integration and phase-related functionalities, due to the high effective mode indexes, waveguides having larger cross-sections compete with waveguides having smaller cross-sections but larger SPP propagation lengths: the figure of merit M_B for a $300 \times 300 \text{ nm}^2$ waveguide is approximately the same as for a $50 \times 150 \text{ nm}^2$ waveguide.

A crucial parameter for the realization of a multi-branched waveguide circuitry is the radius with which it is possible to bend the waveguide, while still having acceptable radiation losses [see an inset to Fig. 3(c)]. This parameter defines the size of all waveguide elements, such as splitters, WRRs, MZIs, etc. The ideal waveguide radius is a trade-off between Ohmic losses (higher for bigger radii) and radiation losses (higher for smaller radii). To determine this radius for each waveguide cross-section a set of 3D propagation-mode numerical simulations has been performed and used to define an all-inclusive figure of merit $M_C = L_{prop}n_{eff}/\lambda d \cdot T/(r/\lambda) = L_{prop}n_{eff}/d \cdot T/r$, where r is the ideal bending radius and T is the corresponding bend transmission. Due to lower values of n_{eff} , waveguides with smaller cross-sections have a low refractive index contrast with the surrounding media. This leads to large radiation losses and consequently large possible bending radii, of the order of several micrometres. Therefore, the behavior of the figure of merit for them is dramatically changed

[Fig. 3(c)], with M_C tending to zero. On the other hand, waveguides with larger cross-sections allow bending radii smaller than a micron (for example for a $300 \times 300 \text{ nm}^2$ waveguide, the ideal bending radius is $r = 0.5 \text{ }\mu\text{m}$). For these waveguides the figure of merit is relatively increased. It should finally be noted that the choice of figure of merit and in particular the weighting factors for its various parameters should be defined by the specific application in mind, e.g., if strong mode confinement is required, it is not necessarily the case that a long propagation length is needed. Thus, if one of the parameters included in the FOM is significantly larger for one of the waveguides, this may completely hide the advantages of another waveguide in terms of a different parameter (c.f. mode area and propagation length).

5. Practical implementation in nanophotonic circuits: materials, GVD and gain

In order to compare various metallic material platforms for Si-based DLSPWs the waveguide guiding properties have been studied for the case of Au, Al, and Cu. The dielectric constants for simulations were taken from Ref. 16, where there are two sets of values for Au and Al depending on different sample preparation and measurement techniques employed in the source references. From Fig. 4 we can conclude that copper is inferior to gold and aluminum in terms of plasmonic properties. Although it provides the highest effective refractive index and the smallest mode area, high Ohmic losses significantly reduce the figure of merit. On the other hand, for the wide range of waveguide cross-sections, the plasmonic properties of aluminum are very similar to those of gold. This makes it a promising candidate for the metallic component of Si-based SPP waveguide circuitry.

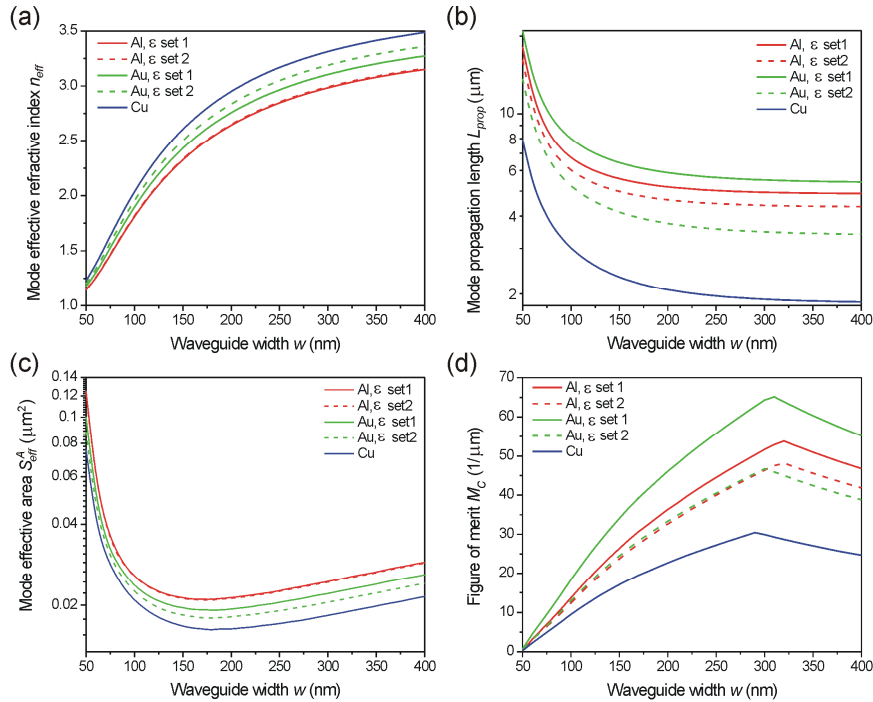


Fig. 4. (a) Effective refractive index, (b) propagation length, (c) effective mode area, and (d) figure of merit M_C for Si-SPP waveguide with height $h = 300 \text{ nm}$ as a function of its width w for various metals: Au, Al and Cu.

Since both Si and metal materials are highly dispersive, and the waveguide dispersion essentially depends on geometrical factors, it is important to estimate the Si-based DLSPW performance for transmitting short pulses. Broadening of the pulse during its propagation is defined by a group velocity dispersion (GVD) parameter $\beta_2 = \partial^2 k_{\text{SPP}} / \partial \omega^2$, which is

presented for the case of a $100 \times 300 \text{ nm}^2$ Si/Al waveguide in the inset to Fig. 1(b). Near telecommunication wavelength of 1550 nm (0.8 eV), β_2 passes zero ensuring a good waveguide performance. The dispersion length for 100 fs pulses is on average 1 mm, which is far beyond the length scale at which these types of waveguide are required. Even at a bit rate of 10 Tb/s, after 5 mode propagation lengths (34 μm) broadening of the pulse is only ~1%. Thus, these waveguides are not dispersion limited. Moreover, the zero-dispersion point is situated at the datacom frequency range [Fig. 1 (b), insert] so that GVD can be further reduced by tuning waveguide geometrical parameters.

For practical implementation in nanophotonic circuits, the Si-based SPP waveguide should be covered with another material, for example silica or polymer. In contradiction with a usual tendency, the propagation length of the mode can be actually increased by coating with material having $n = 1.45$ (from 6.74 μm to 7.57 μm for a $100 \times 300 \text{ nm}^2$ waveguide, remains almost unchanged for a $300 \times 300 \text{ nm}^2$ waveguide). At the same time, the refractive index contrast decreases from 1.81/1 to 2.03/1.45 for a $100 \times 300 \text{ nm}^2$ waveguide and from 2.98/1 to 3.01/1.45 for a $300 \times 300 \text{ nm}^2$ waveguide. In the latter case, the decrease is less dramatic and essentially should not lead to an increase of the waveguide bending radius.

Now we consider the case of coating in connection with possible amplification of the SPP mode propagating in the waveguide. There are two options to introduce the gain medium: using the waveguide core or, alternatively, the waveguide surroundings. The choice of the most efficient approach depends on the waveguide cross-section. For $100 \times 300 \text{ nm}^2$ waveguide, the gain in the core required for lossless propagation of the mode corresponds to $\text{Im}(\varepsilon_{\text{Si}}^*) = 0.14i$, while for active surroundings to $\text{Im}(\varepsilon_{\text{silica}}^*) = 0.03i$. This corresponds to modal gain values of $\sim 1620 \text{ cm}^{-1}$ and $\sim 850 \text{ cm}^{-1}$, respectively. Taking into account that the gain coefficient is proportional to the refractive index of the host medium [18], it can be concluded that the density of active centers (e.g., quantum dots or lasing atoms) required for lossless mode propagation for both options is approximately the same. This should be expected since the energy distribution between the core and the coating is approximately equal. For a $300 \times 300 \text{ nm}^2$ waveguide the situation is different. Most of the mode energy (~90%) is located in the core of the waveguide, so the active coating requires high gain values of $\sim 2.3 \cdot 10^4 \text{ cm}^{-1}$. On the other hand, the gain required in the amplifying core is similar ($\sim 1640 \text{ cm}^{-1}$) to that for the previous cross-section.

6. Conclusion

In conclusion, we have numerically demonstrated efficient singlemode Si-based plasmonic waveguides. The high refractive index of silicon leads to deep subwavelength localization of the photonic signal, higher than in conventional Si-based waveguides, and moreover, to the possibility of sharp (down to 500 nm radius at telecom wavelengths) waveguide bending, important for photonic integration. While the absolute propagation length of the mode is inferior to one in conventional Si-waveguides, for the design of the photonic circuits it is extremely important how strongly the signal is confined within the waveguide and can be affected during propagation by external stimuli. Si-loaded plasmonic waveguides provide unrivalled advantages and are simpler to integrate in CMOS technology than other types of plasmonic waveguide with comparable figures of merit. The M_f figure of merit is the same for Si-loaded SPP waveguides and plasmonic slot waveguides, it is approximately 2 and 3 times smaller than for long-range plasmon waveguides and polymer-based DLSP waveguides, respectively, because of the larger propagation length (while also larger mode area) in the latter cases. An Al/Si material platform ensures good mode propagation parameters and is compatible with CMOS fabrication technology. It is possible, theoretically, to use separations between the waveguides as small as a few tens of nanometres.

To compare waveguide performance in various applications, a set of figures of merits have been developed providing for simple comparisons between both passive and active functionalities. Introduction of gain for achieving lossless SPP propagation is also possible either within the core or surrounding of the proposed guides. We have demonstrated the

potential for on-chip data transfer at rates up to 10 Tb/s, which can be further improved by design of the appropriate waveguide geometry.

Finally, high-refractive index DLSP waveguides can be combined with nonlinear and electro-optical effects. For example, BaTiO₃ thin films possess both high refractive index $n = 2.3$ and a large electro-optic (~ 100 pm/V) and nonlinear optical coefficients. Therefore, BaTiO₃-based SPP waveguides provide a similar level of photonic integration as discussed above for Si-loaded SPP waveguides and can be used for realization of SPP active components, taking advantage of the plasmonic field enhancement.

Acknowledgements

This work was supported by EPSRC (UK) and EC FP6 STREP PLASMOCOM. The authors acknowledge the fruitful discussions with S. I. Bozhevolnyi and W. Dickson.